nature structural & molecular biology

The RNA exosome promotes transcription termination of backtracked RNA polymerase II

Jean-François Lemay[1,4], Marc Larochelle[1,4], Samuel Marguerat[2], Sophie Atkinson[3], Jürg Bähler[3] & François Bachand[1]

The exosome is an RNA-decay complex that constantly monitors transcription and contributes to post-transcriptional turnover of faulty mRNAs. Yet how nuclear RNA surveillance by the exosome is coordinated with transcription is still unknown. Here we show that the RNA exosome of *Schizosaccharomyces pombe* can target the transcription machinery by terminating transcription events associated with paused and backtracked RNA polymerase II (RNAPII); this is contrary to the notion that the exosome acts exclusively on RNAs that have been released by RNAPII. Our data support a mechanism by which RNAPII backtracking provides a free RNA 3′ end for the core exosome, which results in transcription termination with concomitant degradation of the associated transcript. These findings uncover a mechanism of cotranscriptional RNA surveillance whereby termination of transcription by the exosome prevents formation of aberrant readthrough RNAs and transcriptional interference at neighboring genes.

Gene transcription by RNAPII produces a variety of functional transcripts that include mRNA, small nucleolar RNAs (snoRNA) and small nuclear RNAs (snRNA). For a majority of RNAPII-transcribed genes, RNA synthesis involves extensive processing events that occur simultaneously with synthesis[1]. In the case of mRNAs, a nascent precursor mRNA (pre-mRNA) will be processed cotranscriptionally by the addition of a 7-methylguanosine cap at the 5′ end, intron removal, 3′-end endonucleolytic cleavage and polyadenylation. One noteworthy example of coordination between RNA processing and transcription occurs during 3′-end maturation of nascent transcripts, which is coupled to transcription termination[1,2]. Current data suggest a model whereby the cotranscriptional transfer of mRNA 3′ end–processing factors from RNAPII onto the nascent pre-mRNA promotes cleavage at the poly(A) site, providing a free 5′-end entry point for the 5′-3′ exonuclease Rat1 (Xrn2), which is thought to chase RNAPII and promote its dissociation from the DNA template by a mechanism that remains unclear[3–8]. Although this 'torpedo' model of transcription termination depends on prior cleavage of the nascent RNA by 3′ end–processing factors, there is also evidence to support that the transcription process reciprocally influences 3′-end processing. Indeed, RNAPII binding studies show that RNAPII tends to accumulate at the 3′ ends of genes[9–12], suggesting that transcription pauses at or near the poly(A) site to facilitate cleavage-site recognition by the 3′ end–processing factors.

The aforementioned connection between transcription and RNA processing is thought to promote efficient RNA maturation, yet it can also result in inaccurate and unproductive processing events that lead to the expression of defective transcripts. Because the number of mRNA molecules per cell is often low[13], it is clear that errors anywhere in the gene-expression process could have profound consequences on cellular functions. To limit the production of aberrant transcripts, the cell uses a range of surveillance mechanisms, including those of the RNA exosome. The exosome is a conserved RNA-degradation machine that has a fundamental role in monitoring the quality of gene expression in the nucleus. In eukaryotes, the exosome complex is minimally composed of ten evolutionarily conserved subunits, including the catalytically active RNase Dis3 (Rrp44), which exhibits both 3′-5′ exonuclease and endonuclease activities[14,15]. In the yeast nucleus, the core exosome is associated with an additional 3′-5′ exonuclease, Rrp6 (ref. 14). Although early studies suggested that Dis3 and Rrp6 were functionally redundant, the emergence of genetic and biochemical evidence has indicated that they are likely to have different cellular activities[16].

As for RNA maturation, circumstantial evidence suggests that RNA surveillance by the nuclear exosome is also connected to the transcription process[17]. The nuclear exosome in *Drosophila* has been shown to associate directly with the transcription-elongation complex[18]. Studies in *Saccharomyces*, *Chironomus*, *Drosophila* and humans have indicated that the RNA exosome is present at actively transcribed genes[19–22]. Recent results have also suggested that the exosome can influence the transcription process[23–25]. Accordingly, the current view is that the nuclear exosome constantly scrutinizes transcription events and rapidly degrades aberrant RNAs post-transcriptionally. As yet, however, the mechanistic understanding of how the nuclear exosome monitors RNA processing during transcription remains elusive.

To examine this question, we depleted core exosome subunits in the fission yeast *S. pombe* and analyzed the polyadenylated transcriptome and the occupancy profile of RNAPII on a genome-wide scale.

[1]RNA Group, Department of Biochemistry, Université de Sherbrooke, Sherbrooke, Québec, Canada. [2]Medical Research Council Clinical Sciences Centre, Imperial College London, London, UK. [3]Department of Genetics, Evolution and Environment, University College London, London, UK. [4]These authors contributed equally to this work. Correspondence should be addressed to F.B. (f.bachand@usherbrooke.ca).

Received 3 July; accepted 26 August; published online 21 September 2014; doi:10.1038/nsmb.2893

We show that readthrough transcription from many RNAPII-transcribed genes into adjacent genes is prevented by the 3′-5′ exonucleolytic activity of the core exosome. Furthermore, we show that transcription termination defects in exosome-deficient cells depend on TFIIS, a transcription factor that resumes transcription elongation of paused and backtracked RNAPII. Our results support a mechanism of transcription termination whereby RNAPII backtracking at pause sites exposes an unprotected RNA 3′ end that can be targeted by the 3′-5′ exonucleolytic activity of the RNA exosome to promote termination. These findings provide new insights into cotranscriptional RNA surveillance by uncovering a function for the core exosome in a transcription termination pathway that is coupled to RNA decay.

RESULTS

Accumulation of 3′-extended RNAs in exosome-deficient cells

We constructed strains with endogenous *dis3* and *rrp41* genes, which encode core exosome subunits, under the control of the thiamine-repressible *nmt1* promoter (P_{nmt1}). Growing P_{nmt1}-dis3 cells in thiamine-supplemented medium depleted Dis3 by over 85%, resulting in a severe processing defect of a known rRNA substrate (**Supplementary Fig. 1a**,**b**). Notably, depletion of core exosome subunits resulted in the production of 3′-extended mRNAs (**Fig. 1a**, lanes 4 and 6) and snoRNAs (**Supplementary Fig. 1c**,**d**). In contrast, levels of regular-length mRNA were not reduced (**Fig. 1a**), results that do not suggest cleavage defects by the 3′ end–processing machinery. Analysis of Pcf11 recruitment further supports normal 3′-end processing in exosome-deficient cells (**Supplementary Fig. 1e**). Moreover, the 3′-extended mRNAs detected in exosome-depleted cells were cleaved and polyadenylated downstream of *cis* sequences appropriate for 3′-end processing (**Supplementary Fig. 2a**,**b**). We could also detect 3′ extensions just 15 min after exosome inactivation (**Fig. 1b**) when using a previously described temperature-sensitive strain for *dis3* (ref. 26), results suggesting that the 3′-extended transcripts that accumulate in *dis3* and *rrp41* conditional mutants are a direct result of exosome depletion. The RNA-degradation function of the nuclear exosome can be promoted by the activity of an evolutionarily conserved polyadenylation complex, called TRAMP, which in *S. pombe* consists of the RNA helicase Mtr4, the poly(A) polymerase Cid14 and the zinc-knuckle RNA-binding protein Air1 (ref. 27). Interestingly, we did not detect readthrough transcripts in cells deficient for components of the TRAMP complex (**Fig. 1c**,**d**), and readthrough transcripts were not readily detectable in a *rrp6*Δ mutant (**Supplementary Fig. 3**); this suggests a more prominent role for the core exosome relative to the exosome-associated exonuclease Rrp6.

To measure the extent of readthrough-RNA production in exosome-deficient cells, we analyzed the polyadenylated transcriptome of wild-type and mutant cells by strand-specific RNA sequencing (RNA-seq). Consistently with our northern analyses, exosome depletion led to the detection of 3′-extended transcripts expressed from coding and noncoding genes; however, we did not observe these transcripts in Mtr4-depleted cells (**Fig. 2a**). Out of 5,203 genes encoding mRNAs, snoRNAs and snRNAs, 1,692 (33%) and 1,562 (30%) genes showed a significant increase of at least two-fold in the accumulation of 3′-extended transcripts in Dis3- and Rrp41-depleted cells, respectively, with >70% of these genes affected in both mutants ($P < 2.2 \times 10^{-16}$ by one-sided Fisher's exact test). The frequency of readthrough-RNA production in exosome mutants correlated positively with gene expression levels (**Fig. 2b**). The prevalence of 3′-extended transcripts in exosome-deficient cells as identified by RNA-seq can be visualized by plotting cumulative transcript level on the same strand before and after polyadenylation sites (**Fig. 2c**); this level dropped substantially after polyadenylation sites in RNA from wild-type and

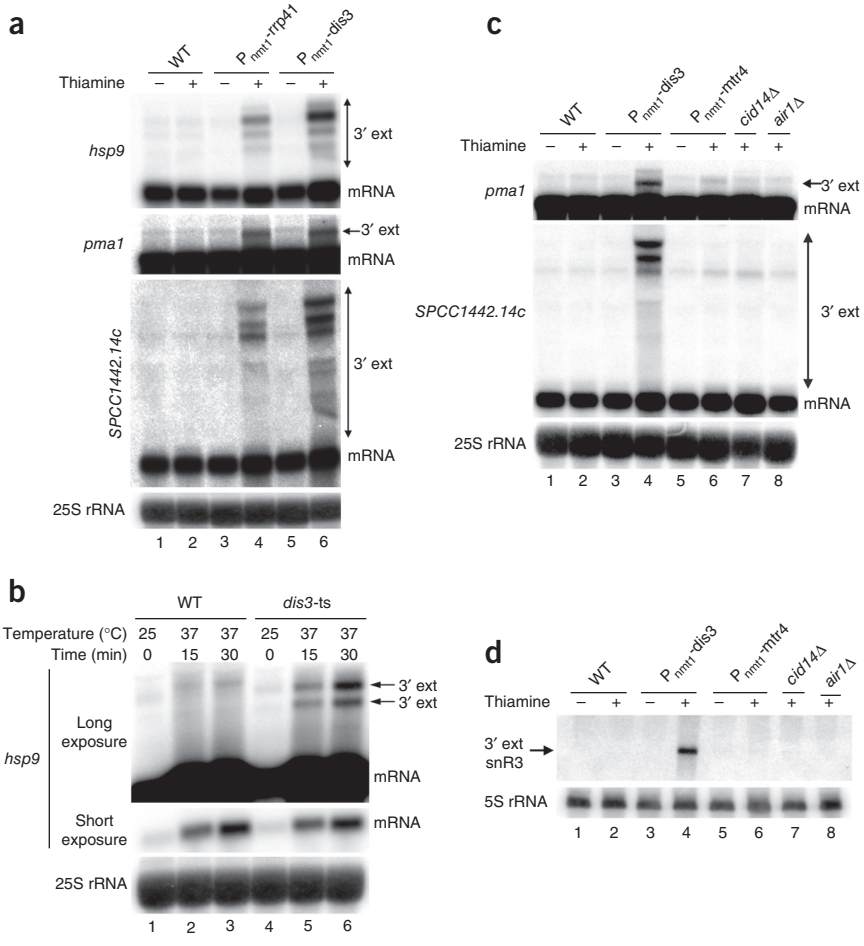

Figure 1 Cells deficient in core exosome subunits, but not the TRAMP complex, accumulate readthrough RNAs. (**a**) Northern analysis of RNA from the indicated strains grown in the absence (–) or presence (+) of thiamine. WT, wild type. 3′ ext, 3′-extended transcripts. (**b**) Northern analysis of *hsp9* mRNA prepared from wild type and temperature-sensitive *dis3* (*dis3*-ts) cells that were grown at the permissive temperature (lanes 1 and 4) or that were shifted to the nonpermissive temperature for 15 min (lanes 2 and 5) or 30 min (lanes 3 and 6). (**c**) Northern analysis of RNA from the indicated strains grown in the absence (–) or presence (+) of thiamine. (**d**) Detection of 3′-extended snR3 transcripts (3′-ext) with an RNA probe complementary to the RNase H–cleaved product. Samples are equal amounts of total RNA extracted from the indicated strains grown in the absence (–) or in the presence (+) of thiamine and treated with RNase H in the presence of DNA oligonucleotides complementary to snR3 transcripts present beyond the poly(A) site. The positions of the DNA oligonucleotides used are shown in **Supplementary Figure 1c**. Uncropped images of the blots are shown in **Supplementary Data Set 1**.

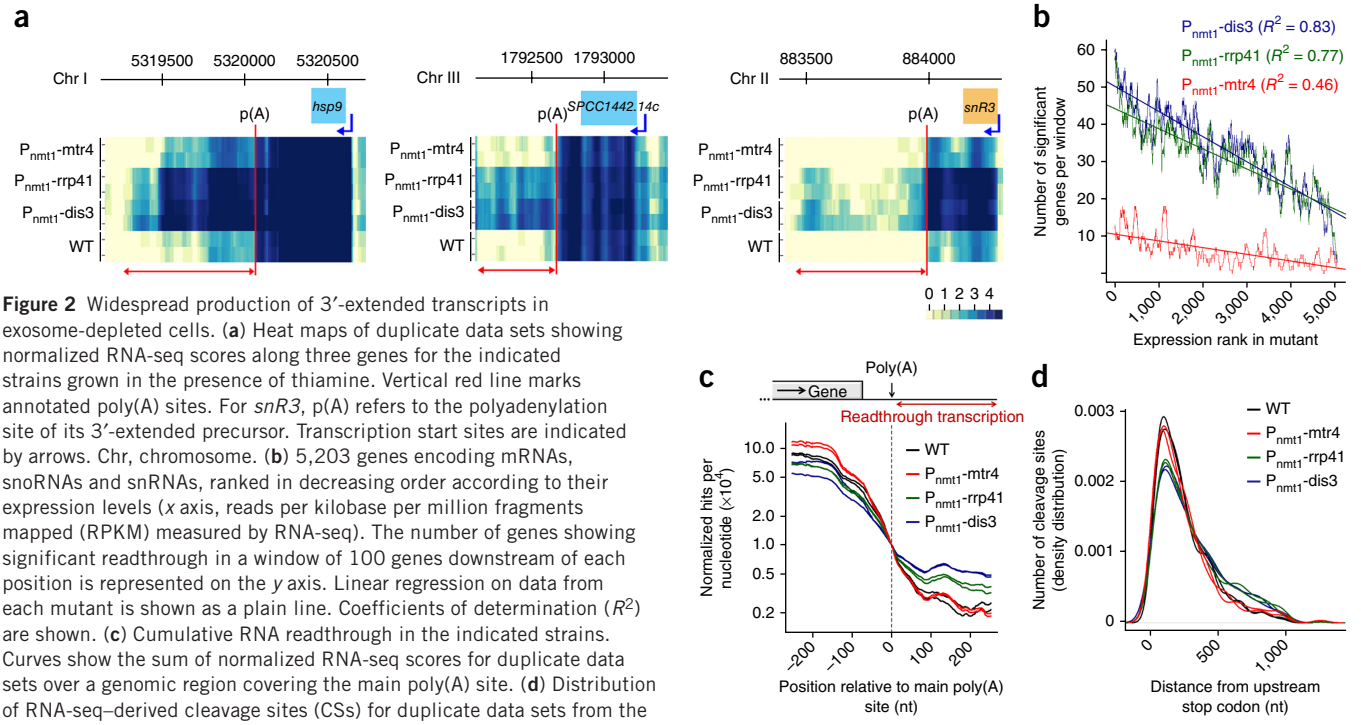

Figure 2 Widespread production of 3′-extended transcripts in exosome-depleted cells. (**a**) Heat maps of duplicate data sets showing normalized RNA-seq scores along three genes for the indicated strains grown in the presence of thiamine. Vertical red line marks annotated poly(A) sites. For *snR3*, p(A) refers to the polyadenylation site of its 3′-extended precursor. Transcription start sites are indicated by arrows. Chr, chromosome. (**b**) 5,203 genes encoding mRNAs, snoRNAs and snRNAs, ranked in decreasing order according to their expression levels (*x* axis, reads per kilobase per million fragments mapped (RPKM) measured by RNA-seq). The number of genes showing significant readthrough in a window of 100 genes downstream of each position is represented on the *y* axis. Linear regression on data from each mutant is shown as a plain line. Coefficients of determination (R^2) are shown. (**c**) Cumulative RNA readthrough in the indicated strains. Curves show the sum of normalized RNA-seq scores for duplicate data sets over a genomic region covering the main poly(A) site. (**d**) Distribution of RNA-seq–derived cleavage sites (CSs) for duplicate data sets from the indicated strains with respect to the upstream stop codon. Mapped CSs in exosome mutants, as compared to wild-type cells, are on average significantly more distant from the stop codon ($P < 3.2 \times 10^{-5}$ ($n = 648$ 3′-untranslated-region coordinates) and $P < 2.2 \times 10^{-3}$ ($n = 304$) for *dis3*; $P < 1.1 \times 10^{-4}$ ($n = 600$) and $P < 4.9 \times 10^{-6}$ ($n = 728$) for *rrp41* by Wilcoxon rank-sum test). No significant change was found for Mtr4-depleted cells. Experiments were performed in biological duplicates (independent cell cultures).

Mtr4-depleted cells but remained high in Dis3- and Rrp41-depleted cells. Consistently with this observation, the distribution of mapped cleavage sites indicated that distal poly(A) sites were more frequently used in exosome mutants than in wild-type cells (**Fig. 2d**). Collectively, these results indicate that loss of exosome function results in the widespread production of 3′-extended transcripts.

RNAPII termination defects in exosome-depleted cells

At least two different mechanisms could account for the increased production of 3′-extended transcripts in exosome-deficient cells: post-transcriptional turnover of aberrant readthrough RNAs[28,29] and/or a role for the exosome in transcription termination. If all of the 3′-extended transcripts detected in exosome-deficient cells originate from the stabilization of constitutively transcribed readthrough RNAs, no change in RNAPII occupation across genes would be expected after loss of exosome function. Yet if the core exosome is involved in transcription termination, increased levels of RNAPII density should be detected at the 3′ ends of genes. To measure RNAPII density along genes, we performed chromatin immunoprecipitation (ChIP) assays with an antibody (8WG16) that recognizes the C-terminal domain (CTD) of RNAPII and analyzed immunoprecipitates by high-throughput sequencing (ChIP-seq). Analysis of RNAPII density at a snoRNA (**Fig. 3a**) and an mRNA (**Fig. 3b**) gene that showed accumulation of 3′-extended transcripts in exosome mutants (**Figs. 1** and **2**) revealed greater RNAPII cross-linking at the 3′ end in Dis3- and Rrp41-depleted cells relative to the wild-type. Accordingly, transcription through the *SPCC1442.14c* terminator region (**Fig. 3b**) resulted in the production of chimeric *SPCC1442.14c-SPCC1442.13c* transcripts in exosome-deficient cells (**Supplementary Fig. 2c**). Importantly, transcription termination defects are a general feature of exosome-depleted cells, as shown in the plot of cumulative levels of RNAPII binding relative to annotated cleavage sites, which indicated a clear shift in RNAPII density downstream of the noticeable decline observed in wild-type cells (**Fig. 3c**). The genome-wide increase in readthrough transcription was also evident in a CTD-independent ChIP approach that used an antibody to the hemagglutinin (HA) tag of a core RNAPII component (Rpb3-HA; **Fig. 3d**). Several classes of RNAPII-transcribed genes showed a 3′-extended profile of RNAPII cross-linking in exosome mutants, including mRNA-, snoRNA- and snRNA-encoding genes (**Supplementary Fig. 4a**) as well as both tandem and convergent gene pairs (**Supplementary Fig. 4b**). We also detected exosome-dependent transcription termination defects with a reporter-gene assay in which the transcription termination element of the *snR99* (official symbol *sno12*) gene was inserted upstream of the *ura4* gene (**Supplementary Fig. 4c–h**). We also measured the distribution of actively elongating RNAPII by transcription run-on (TRO) assays on the *pma1* (**Fig. 3e**) and *snR3* (**Fig. 3h**) loci. In agreement with the ChIP-seq data, TRO assays revealed increased production of nascent RNA at the 3′ end in Dis3- and Rrp41-depleted cells (**Fig. 3f,i**). Therefore, a substantial proportion of RNAPII that terminates downstream of *pma1* and *snR3* coding regions in wild-type cells fails to terminate in exosome mutants (**Fig. 3g,j**), thus indicating that the readthrough transcripts detected in exosome mutants are caused by a termination defect and not simply by RNA stabilization. Collectively, the widespread detection of 3′-extended transcripts in exosome-deficient cells as determined by RNA-seq together with the global increase in RNAPII density at the 3′ ends of genes supports the idea that the exosome functions in RNAPII termination.

The *S. pombe* exosome is present at RNAPII-transcribed genes

To begin to explore the mechanism by which the RNA exosome promotes transcription termination, we first assessed whether subunits of the core exosome complex were associated with sites of RNAPII transcription by ChIP assays, which have previously been used to show the presence

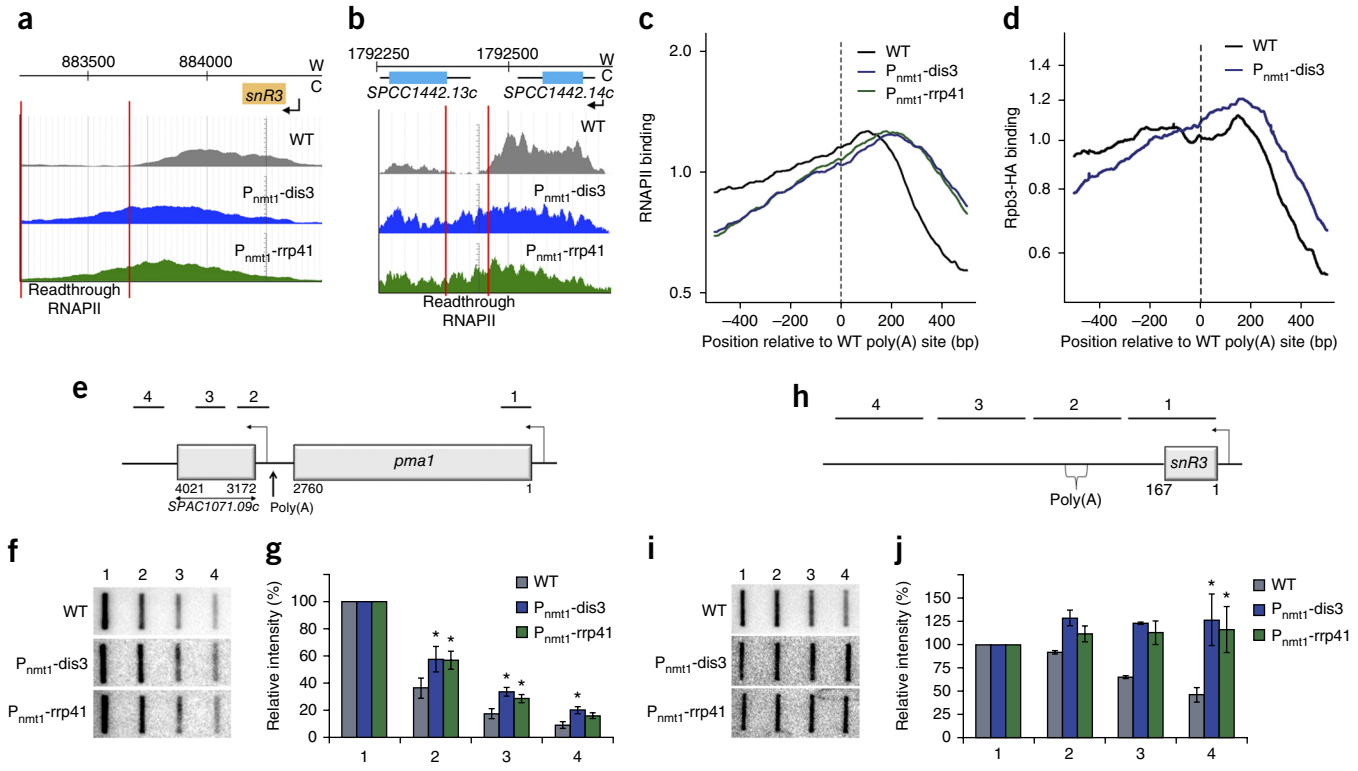

Figure 3 The core exosome promotes termination of RNAPII transcription. (**a**,**b**) RNAPII profiles (ChIP-seq) across the *snR3* (**a**) and *SPCC1442.14c* (**b**) genes in the indicated strains. W, Watson strand; C, Crick strand. (**c**,**d**) Cumulative Rpb1 (**c**) and Rpb3-HA (**d**) profiles relative to poly(A)–cleavage sites in the indicated strains. Curves show the sum of normalized ChIP-seq sequencing scores over a genomic region covering the main poly(A) site. (**e**,**h**) Schematic showing the position of probes used for transcription run-on (TRO) assays on *pma1* (**e**) and *snR3* (**h**) genes. (**f**,**i**) TRO blots (representative of three total) for *pma1* (**f**) and *snR3* (**i**). Uncropped images of the blots are shown in **Supplementary Data Set 1**. (**g**,**j**) Quantification of TRO analyses for *pma1* (**g**) and *snR3* (**j**) genes. Transcription levels were corrected for background signal and plotted as a percentage relative to probe 1. Error bars in **g** indicate s.d. ($n = 3$ biological replicates from independent cell cultures). $^*P < 0.05$ (two-tailed Student's *t* test). Bars in **j** indicate either the range (probes 2 and 3) of measured values from $n = 2$ independent experiments or s.d. (probes 1 and 4) from $n = 3$ biological replicates from independent cell cultures. $^*P < 0.05$ (two-tailed Student's *t* test).

of exosome subunits at actively transcribed genes in *Saccharomyces cerevisiae*[21], *Drosophila*[18] and humans[19]. Consistently with these observations, ChIP assays with tagged versions of Dis3, Rrp41, Csl4 and Rrp4 showed that these four exosome subunits are associated with sites of snoRNA and mRNA transcription (**Fig. 4a**,**b**). Importantly, exosome recruitment to a gene is dependent on active transcription: Dis3 levels at the *nmt1* gene were reduced in conditions that repress *nmt1* transcription (**Fig. 4c**; +thiamine), whereas Dis3 levels at the *hsp9* gene were increased in conditions that activate *hsp9* expression (**Fig. 4d**; +cadmium). Thus, our data indicate that in fission yeast, as in the aforementioned species[18,19,21], the exosome is present along actively transcribed genes, supporting the involvement of the exosome in transcription termination.

Dis3 3′-5′ exonucleolytic activity is necessary for termination

The single catalytic subunit of the core exosome, Dis3, catalyzes both 3′-5′ exonucleolytic and endonucleolytic RNA cleavage[14,15]. Endonucleolytic cleavage by the RNA exosome could promote transcription termination by a mechanism similar to the termination pathway triggered by the endonucleolytic cleavage catalyzed by the 3′-end mRNA-processing machinery[2]. To test this possibility, we generated *dis3* alleles expressing single amino acid substitutions at conserved aspartate residues (**Supplementary Fig. 5a**) that were previously shown in *S. cerevisiae* to be devoid of exonucleolytic or endonucleolytic activities[30]. We chromosomally integrated the different *dis3* alleles as single copies into the P_{nmt1}-dis3 conditional strain and confirmed that they were expressed at levels similar to those in wild-type Dis3 (**Supplementary Fig. 5b**). After repression of endogenous *dis3* by thiamine, the expression of wild-type as well as endonucleolytic (endo$^-$), exonucleolytic (exo$^-$) and double (endo$^-$ exo$^-$) mutant versions of *S. pombe* Dis3 resulted in growth phenotypes (**Supplementary Fig. 5c**,**d**) similar to the phenotypes of the corresponding *S. cerevisiae dis3* mutants[30,31]. We next used RNAPII ChIP assays to examine the extent to which the endo$^-$ and exo$^-$ versions of Dis3 restored the transcription termination defects induced by the depletion of endogenous Dis3. As a control, expression of wild-type Dis3 in the P_{nmt1}-dis3 strain prevented the thiamine-dependent increase in RNAPII levels downstream of genes (**Fig. 5a–d**). Strikingly, whereas the endonucleolytically deficient version of Dis3 fully restored RNAPII density downstream of the *snR3* and *pma1* genes, the exonuclease mutant showed a significant increase in RNAPII density at the 3′ ends of genes (**Fig. 5c**,**d**). Consistently with these RNAPII ChIP data, RNA analysis showed the accumulation of 3′-extended transcripts in cells that expressed the exonuclease-deficient version of Dis3 but not in cells expressing the endonucleolytically inactive version (**Supplementary Fig. 5e**). These results indicate that the 3′-5′ exonucleolytic activity, but not the endonucleolytic activity, of Dis3 is required for exosome-dependent transcription termination.

The central channel is required for RNAPII termination

We also examined whether access through the exosome central channel was required for transcription termination by introducing an 11-residue insertion in Rrp41 (**Supplementary Fig. 6a**) that impedes

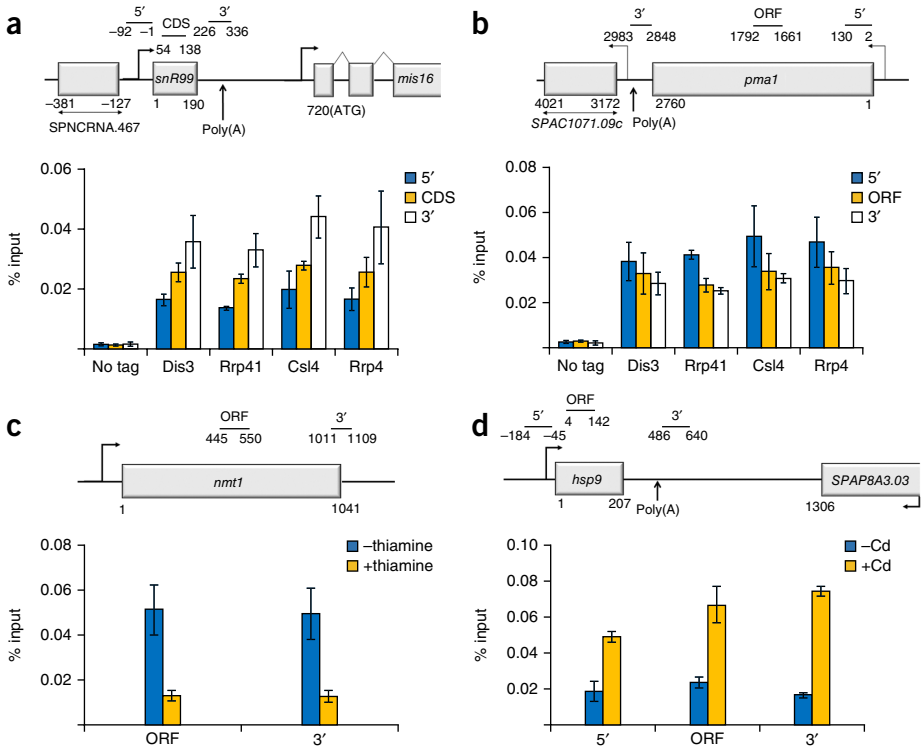

Figure 4 Transcription-dependent recruitment of core exosome subunits to genes. (**a**,**b**) Top, schematic of *snR99* snoRNA (**a**) and *pma1* mRNA (**b**) genes. Bars above the genes show the positions of PCR products used for ChIP analyses. Bottom, quantitative PCR (qPCR) of coprecipitated DNA from ChIP assays performed with tandem affinity purification (TAP)-tagged versions of Dis3, Rrp41, Csl4 and Rrp4 as well as with an untagged control strain. qPCR results for the *snR99* (**a**) and *pma1* (**b**) genes are shown. CDS, coding sequence; ORF, open reading frame. (**c**) ChIP assays with extracts of cells that expressed Dis3-TAP and that were previously grown in the absence (–) or presence (+) of thiamine. Bar graph, input and coprecipitated DNA quantified by qPCR along the *nmt1* gene with specific primers shown in schematic above the graph. (**d**) ChIP assays with extracts of cells that expressed Dis3-TAP and that were previously grown in the absence (–) or presence (+) of 1 mM cadmium (Cd) for 60 min. Bar graph, input and coprecipitated DNA quantified by qPCR along the *hsp9* gene with specific primers shown in schematic above the graph. Bars indicate either the range of measured values from two independent experiments (**d**) or the s.d. (**a**–**c**) from three experiments with independent cell cultures.

RNA from threading through the channel[32]. After repression of endogenous Rrp41 by thiamine, expression of the *rrp41* mutant allele into the P_{nmt1}-rrp41 conditional strain failed to support the essential functions of the RNA exosome (**Supplementary Fig. 6b**,**c**) but did not impair exosome assembly (**Supplementary Fig. 6d**). Importantly, blocking the channel of the RNA exosome resulted in readthrough transcription (**Fig. 5e**,**f**), thus indicating that passage through the central channel is required for transcription termination by the core exosome.

Exosome-dependent termination involves RNAPII backtracking

Because transcription termination by the exosome requires a functional exonuclease domain, a free single-stranded 3′-end substrate must be available in the context of the transcription process. One transcriptional state in which a free single-stranded RNA 3′ end can be accessible occurs on arrested and backtracked RNAPII (ref. 33). During backtracking, the catalytic site of RNAPII becomes disengaged from the RNA 3′ end, and RNAPII moves backward, causing the 3′ end of the nascent RNA to extrude out of the polymerase through the secondary channel[34]. Backtracked RNAPII can be rescued by the slow intrinsic hydrolyzing activity of RNAPII, which is stimulated by the transcription factor TFIIS[35] (Tfs1 in *S. pombe*) and which cleaves the extruded RNA and causes the realignment of the RNA 3′ end in the catalytic site, allowing transcription to resume. We thus hypothesized that exosome-mediated transcription termination depends on RNAPII backtracking, whereby

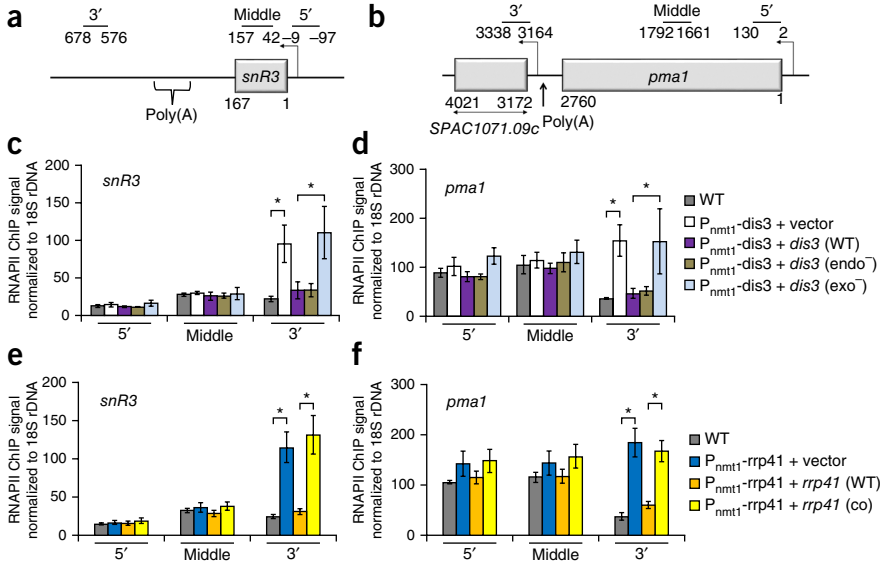

Figure 5 The 3′-5′ exonucleolytic activity of Dis3 and the exosome central channel are required for transcription termination. (**a**,**b**) Schematic representation of *snR3* snoRNA (**a**) and *pma1* mRNA (**b**) genes. Bars above the genes show the positions of PCR products used for ChIP analyses in **c**–**f**. (**c**,**d**) ChIP analysis of RNAPII density along the *snR3* (**c**) and *pma1* (**d**) genes (5′ end, middle and 3′ end). Samples are extracts prepared from the P_{nmt1}-dis3 conditional strain that was previously transformed with constructs expressing wild-type Dis3 (WT), an endonuclease-deficient Dis3 (endo⁻), a 3′-5′ exonuclease–deficient Dis3 (exo–) or the vector control. (**e**,**f**) ChIP analysis of RNAPII along the *snR3* (**e**) and *pma1* (**f**) genes. Samples are extracts prepared from the P_{nmt1}-rrp41 conditional strain that was previously transformed with constructs expressing wild-type Rrp41 (WT), the channel-occluded (co) version of Rrp41 or the empty vector control. The wild-type strain was also analyzed as a control in thiamine-supplemented medium. Error bars, s.d. ($n = 3$ biological replicates from independent cell cultures). $^*P < 0.05$ (two-tailed Student's t test).

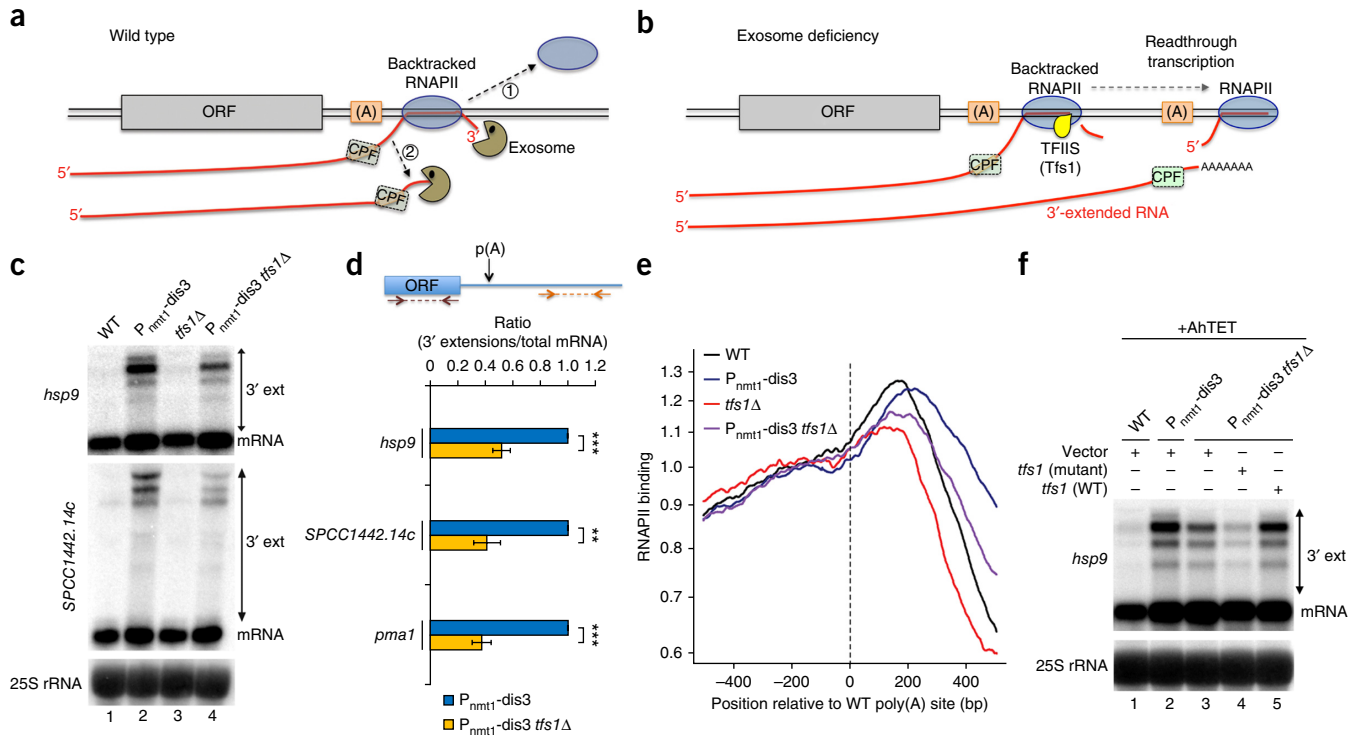

Figure 6 Transcription termination by the exosome is mechanistically linked to RNAPII backtracking. (**a**) Model in which backtracking provides a free RNA 3′ end for the core exosome, promoting termination (1) and degradation (2) of potential readthrough RNAs uncleaved by the cleavage and polyadenylation factor (CPF) machinery. (A), poly(A) site. (**b**) In exosome mutants, TFIIS (Tfs1 in *S. pombe*)-stimulated RNAPII-mediated RNA cleavage outcompetes termination of backtracked RNAPII by the exosome, allowing transcription to resume until 3′-end processing at distal cleavage sites. (**c**) Northern analysis of RNA from the indicated strains grown in the presence of thiamine. (**d**) Ratio of 3′-extended transcripts relative to total mRNA as measured by real-time PCR (rt-PCR) with primers located downstream of poly(A) sites and in ORF sequences. Data in the P_{nmt1}-dis3 *tfs1*Δ double mutant are relative to the single P_{nmt1}-dis3 mutant. Error bars, s.d. ($n = 3$ biological replicates from independent cell cultures). $^{**}P < 0.01$; $^{***}P < 0.001$ (two-tailed Student's *t* test). (**e**) Cumulative RNAPII profile in the indicated strains. Curves show the sum of normalized ChIP-seq sequencing scores over a genomic region covering the main poly(A) site. (**f**) Northern analysis of RNA from wild type, P_{nmt1}-dis3 and P_{nmt1}-dis3 *tfs1*Δ cells transformed with an expression vector for wild-type (lane 5) or mutant (lane 4) Tfs1 under the control of tetracycline (AhTET) or empty vector (lanes 1–3). Cells were grown for 6 h in the presence of thiamine, after which AhTET was added for another 6 h. Uncropped images of gels are shown in **Supplementary Data Set 1**.

extrusion of the nascent RNA provides a substrate for the core exosome, triggering polymerase release and the concomitant degradation of the readthrough RNA (**Fig. 6a**). In exosome-depleted cells (**Fig. 6b**), TFIIS would outcompete exosome-mediated termination, promoting the reactivation of backtracked RNAPII complexes until they were to reach distal contexts for 3′-end processing and polyadenylation, thus resulting in the production of readthrough transcripts.

To test this model, we deleted *tfs1* (TFIIS) in wild-type and P_{nmt1}-dis3 cells. The absence of Tfs1 in exosome-depleted cells resulted in reduced levels of readthrough RNAs relative to the single exosome mutant (**Fig. 6c**, comparison of lanes 2 and 4). In contrast, levels of regular-length mRNAs were not affected (**Fig. 6c**), thus indicating that the absence of Tfs1 specifically reduced the levels of readthrough transcripts relative to regular mRNAs in Dis3-depleted cells (**Fig. 6d**). To support these RNA analyses, we examined RNAPII profiles by ChIP-seq. The absence of TFIIS in *S. pombe* did not impair RNAPII occupancy in the coding regions (**Fig. 6e**, comparison of red and black profiles upstream of the poly(A) site). This observation is consistent with the absence of a detectable decrease in mRNA levels in *tfs1*Δ cells (**Fig. 6c**) and with data from TFIIS mutants in *S. cerevisiae*[36,37]. The absence of Tfs1 resulted in premature dissociation of RNAPII downstream of poly(A) sites in contrast to coding regions (**Fig. 6e**, comparison of red and black profiles downstream of the poly(A) site). Importantly, premature termination in the *tfs1*Δ mutant required the RNA exosome, because depletion of Dis3 suppressed the earlier-termination phenotype seen in the *tfs1*Δ single mutant (**Fig. 6e**, comparison of red and purple profiles). Likewise, the absence of Tfs1 suppressed readthrough transcription in Dis3-depleted cells (**Fig. 6e**, comparison of blue and purple profiles). These data suggest that the RNA exosome and TFIIS compete for backtracked RNAPII at the 3′ ends of genes.

Even in the absence of TFIIS, arrested and backtracked RNAPII can be reactivated by the intrinsic RNA-cleavage activity of the polymerase large subunit, albeit less efficiently[37]. We therefore tested the effect of a previously described mutant of TFIIS that inhibits the cleavage activity of RNAPII and prevents the rescue of backtracked transcription complexes[37] (**Supplementary Fig. 7a**,**b**). Notably, expression of this dominant-negative TFIIS mutant almost completely abolished the production of exosome-dependent readthrough transcripts (**Fig. 6f**, comparison of lane 4 to lanes 1 and 2; quantification in **Supplementary Fig. 7c**), thus indicating that the remaining readthrough RNAs produced in the absence of Tfs1 (**Fig. 6c**, lane 4, and **Fig. 6f**, lane 3) result from the nonstimulated intrinsic cleavage activity of RNAPII. As a control, expression of wild-type Tfs1 in the P_{nmt1}-dis3 *tfs1*Δ double-mutant strain restored the levels of readthrough RNA detected in the single P_{nmt1}-dis3 mutant (**Fig. 6f**, comparison of lane 5 to lane 2). Together, these results indicate that the detection of 3′-extended RNAs and readthrough RNAPII in exosome-depleted cells depends on TFIIS. Given the established role of TFIIS in the reactivation of backtracked RNAPII *in vitro* and

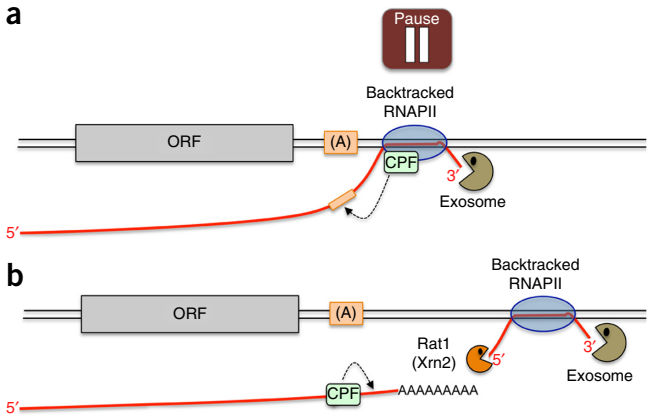

Figure 7 Model of cotranscriptional RNA surveillance by the RNA exosome by competition with 3′-end processing. (**a**) Transcriptional pausing, which is frequently associated with RNAPII backtracking[33,38], enhances 3′-end processing by the cleavage and polyadenylation factor (CPF) complex by facilitating the recognition of poly(A) signals on the nascent transcripts. RNAPII backtracking also provides a free RNA 3′ end for exosome-dependent termination, thereby challenging the CPF complex to efficiently process the nascent pre-mRNA. In the case of unproductive cleavage by the CPF, exosome-dependent termination would promote the removal of backtracked RNAPII together with the degradation of the uncleaved transcripts (**Fig. 6a**), thereby preventing the potential for readthrough transcription. (**b**) Productive 3′-end processing by the CPF releases the pre-mRNA for polyadenylation and provides a substrate for the 5′-3′ exonuclease Rat1 (Xrn2) to promote termination of transcription.

in vivo[34,37,38], we conclude that exosome-mediated transcription termination involves RNAPII backtracking.

Backtracking is a major mechanism underlying pausing of RNA polymerases[38]. We therefore tested the impact of mutations at the 3′ end of the *ura4* gene (**Supplementary Fig. 7d**) that perturb RNAPII pausing[39] on exosome-dependent termination. Consistently with previous findings[39], removal of these transcriptional pause signals resulted in transcription termination defects, as measured by the four-fold increase in RNAPII density at the 3′ end of the mutant *ura4* gene relative to wild-type *ura4* (**Supplementary Fig. 7e**). Next, we chromosomally integrated wild-type and mutant *ura4* constructs into the P_{nmt1}-dis3 conditional strain and measured RNAPII density at the 3′ end of *ura4* by ChIP assays on cells cultured in the presence or absence of thiamine. Consistently with our previous results, we found a thiamine-dependent increase in RNAPII density at the 3′ end of the wild-type *ura4* gene in P_{nmt1}-dis3 cells relative to control cells (**Supplementary Fig. 7f**, wild-type *ura4* 3′). In contrast, readthrough polymerases that result from loss of exosome function were no longer detected at the 3′ end of the pause-defective *ura4* mutant (**Supplementary Fig. 7f**, mutant *ura4* 3′). Together, these results indicate that transcription termination by the RNA exosome is mechanistically linked to RNAPII pausing and backtracking.

DISCUSSION

In this study, we identified an unexpected role for the RNA exosome in a transcription termination pathway coupled to RNAPII pausing and arrest. We provide evidence into how this termination-coupled RNA-degradation pathway promotes the removal of backtracked RNAPII, thereby preventing the production of readthrough transcripts and transcription interference into neighboring genes. These findings provide mechanistic insights into the cross-talk between RNA surveillance, 3′-end processing, and transcription termination.

Termination of backtracked RNAPII by the RNA exosome

Genome-wide studies indicate that transcription elongation by RNAPII is not a uniform process[40] but that RNAPII frequently pauses and backtracks after facing obstacles in the template DNA, such as nucleosomes[38]. Reactivation of backtracked polymerase by TFIIS-stimulated RNA cleavage is a mechanism known to resume transcription elongation by RNAPII[34,40]. In principle, a backtracked RNAPII complex could also be removed by disassembling the arrested polymerase to result in termination. However, although *in vitro* work has underscored the importance of backtracking in transcription termination by eukaryotic RNA polymerase III (ref. 41) and the prokaryotic RNA polymerase[42], experimental evidence associating polymerase backtracking and transcription termination has not been reported for RNAPII. Our results now provide evidence that the RNA exosome can terminate transcription events associated with backtracked RNAPII. Although the nature of the obstructions promoting RNAPII backtracking at the ends of genes remains to be determined, pausing of RNAPII downstream of poly(A) signals has been supported by several studies[9–12] and is consistent with the accumulation of RNAPII beyond annotated poly(A) sites in our ChIP-seq analyses (**Fig. 3**, **Supplementary Fig. 4** and **Fig. 6**). Backtracking at pause sites can extend to dozens of nucleotides in a biological context[38], a length sufficient to extrude RNA from the funnel-shaped pore of RNAPII[34] and expose an unprotected single-stranded RNA 3′ end. Threading of such single-stranded RNA by the unwinding substrate-entry pore of the core exosome[43] would allow the RNA to reach the Dis3 active site for processive 3′-5′ exonucleolytic activity, which may displace the paused and less stable polymerase complex. Alternatively, the processive exonucleolytic activity of the exosome may promote further backtracking once the exosome reaches the polymerase, and this could trigger hairpin-dependent termination[41]. Thus, in addition to proteasome-dependent degradation of RNAPII (ref. 44), exosome-dependent termination provides an additional means to control transcriptional arrest when reactivation mechanisms are not desired.

RNA surveillance by the exosome via termination-coupled RNA decay

Accumulating evidence supports that poly(A)-dependent 3′-end processing is coupled to transcription termination. Nevertheless, a substantial fraction of RNAPII fails to terminate upon reaching a poly(A) signal[2], presumably owing to nonproductive endonucleolytic cleavage by the 3′ end–processing machinery. Although such readthrough transcription is known to be coupled to exosome-mediated RNA degradation[29,45], it was unclear how the RNA exosome post-transcriptionally distinguishes readthrough transcripts from normal mRNAs. The results presented in this study support the idea that termination-coupled RNA degradation by the exosome competes with 3′-end processing when RNAPII pauses and backtracks downstream of poly(A) signals (**Fig. 7a**). In productive cases, 3′-end cleavage would occur, and the exosome-dependent termination pathway uncovered in this study would not have access to the pre-mRNA because the pre-mRNA is physically separated from the arrested transcription complex, owing to 3′-end cleavage and polyadenylation (**Fig. 7b**). Furthermore, in the case of productive 3′-end processing, we suggest a double torpedo model of transcription termination, whereby the 3′-5′ exonucleolytic activity of the core exosome might cooperate with the 5′-3′ exonuclease activity of the Rat1 (Xrn2) complex to disengage RNAPII from the DNA template (**Fig. 7b**). In contrast, in the case in which 3′-end processing does not result in productive endonucleolytic cleavage, the core exosome could promote transcription termination and degrade the uncleaved aberrant pre-mRNA (**Fig. 6a**). By competing with mRNA 3′-end processing, transcription termination

by the RNA exosome may provide a failsafe mechanism that promotes the removal of paused and backtracked RNAPII associated with uncleaved transcripts (**Fig. 6a**), thereby preventing the potential for readthrough transcription via reactivation of arrested RNAPII (**Fig. 6b**).

In summary, our findings provide evidence for a new mechanism of transcription termination coupled to RNAPII backtracking that functions in cotranscriptional RNA surveillance by the nuclear exosome. Because backtracked RNAPII is a proposed entry point for the human exosome during class-switch recombination at transcribed immunoglobulin loci[19], we predict that the mechanism described in this study highlights a general feature of cotranscriptional nuclear surveillance in eukaryotes.

METHODS

Methods and any associated references are available in the online version of the paper.

Accession codes. RNA-seq and ChIP-seq data have been deposited in the ArrayExpress database under accession number E-MTAB-2237.

Note: Any Supplementary Information and Source Data files are available in the online version of the paper.

ACKNOWLEDGMENTS

We thank M. Bühler and P.-E. Jacques for helpful discussions; M. Yamamoto (University of Tokyo) and D. Hermand (University of Namur) for strains; M. Durant and E. Lapointe (both at Laboratoire de Génomique Fonctionnelle de l'Université de Sherbrooke) for ChIP-seq libraries; M. Luetzelberger (University of Braunschweig) for the tetracycline-inducible expression vector; the sequencing platform of the McGill University and Génome Québec Innovation Centre; and S. Abou Elela, E. Lei and A. Morillon for critical reading of the manuscript. This work was supported by funding from the Natural Sciences and Engineering Research Council of Canada (NSERC) to F.B., from a Wellcome Trust Senior Investigator Award to J.B. and from the UK Medical Research Council to S.M. J.-F.L. was supported by an Alexander Graham-Bell Doctoral Scholarship from NSERC. F.B. is supported as a Canada Research Chair in Quality Control of Gene Expression.

AUTHOR CONTRIBUTIONS

J.-F.L., M.L. and F.B. conceived and designed the research project; J.-F.L. and M.L. performed the experiments; S.M. and S.A. prepared the RNA-seq libraries in collaboration with J.B.; S.M. performed computational analyses of RNA-seq and ChIP-seq experiments; J.-F.L., M.L., S.M. and F.B. analyzed the data; F.B. wrote the manuscript; and all authors discussed the results and commented on the manuscript.

COMPETING FINANCIAL INTERESTS

The authors declare no competing financial interests.

1. Bentley, D.L. Coupling mRNA processing with transcription in time and space. *Nat. Rev. Genet.* **15**, 163–175 (2014).
2. Mischo, H.E. & Proudfoot, N.J. Disengaging polymerase: terminating RNA polymerase II transcription in budding yeast. *Biochim. Biophys. Acta* **1829**, 174–185 (2013).
3. Dengl, S. & Cramer, P. Torpedo nuclease Rat1 is insufficient to terminate RNA polymerase II *in vitro*. *J. Biol. Chem.* **284**, 21270–21279 (2009).
4. Jimeno-González, S., Schmid, M., Malagon, F., Haaning, L.L. & Jensen, T.H. Rat1p maintains RNA polymerase II CTD phosphorylation balance. *RNA* **20**, 551–558 (2014).
5. Kim, M. *et al.* The yeast Rat1 exonuclease promotes transcription termination by RNA polymerase II. *Nature* **432**, 517–522 (2004).
6. Luo, W., Johnson, A.W. & Bentley, D.L. The role of Rat1 in coupling mRNA 3′-end processing to transcription termination: implications for a unified allosteric-torpedo model. *Genes Dev.* **20**, 954–965 (2006).
7. Pearson, E.L. & Moore, C.L. Dismantling promoter-driven RNA polymerase II transcription complexes *in vitro* by the termination factor Rat1. *J. Biol. Chem.* **288**, 19750–19759 (2013).
8. West, S., Gromak, N. & Proudfoot, N.J. Human 5′ → 3′ exonuclease Xrn2 promotes transcription termination at co-transcriptional cleavage sites. *Nature* **432**, 522–525 (2004).
9. Anamika, K., Gyenis, A., Poidevin, L., Poch, O. & Tora, L. RNA polymerase II pausing downstream of core histone genes is different from genes producing polyadenylated transcripts. *PLoS ONE* **7**, e38769 (2012).
10. Coudreuse, D. *et al.* A gene-specific requirement of RNA polymerase II CTD phosphorylation for sexual differentiation in *S. pombe*. *Curr. Biol.* **20**, 1053–1064 (2010).
11. Glover-Cutter, K., Kim, S., Espinosa, J. & Bentley, D.L. RNA polymerase II pauses and associates with pre-mRNA processing factors at both ends of genes. *Nat. Struct. Mol. Biol.* **15**, 71–78 (2008).
12. Gromak, N., West, S. & Proudfoot, N.J. Pause sites promote transcriptional termination of mammalian RNA polymerase II. *Mol. Cell. Biol.* **26**, 3986–3996 (2006).
13. Marguerat, S. *et al.* Quantitative analysis of fission yeast transcriptomes and proteomes in proliferating and quiescent cells. *Cell* **151**, 671–683 (2012).
14. Chlebowski, A., Lubas, M., Jensen, T.H. & Dziembowski, A. RNA decay machines: the exosome. *Biochim. Biophys. Acta* **1829**, 552–560 (2013).
15. Schneider, C. & Tollervey, D. Threading the barrel of the RNA exosome. *Trends Biochem. Sci.* **38**, 485–493 (2013).
16. Januszyk, K. & Lima, C.D. The eukaryotic RNA exosome. *Curr. Opin. Struct. Biol.* **24**, 132–140 (2014).
17. Schmid, M. & Jensen, T.H. Transcription-associated quality control of mRNP. *Biochim. Biophys. Acta* **1829**, 158–168 (2013).
18. Andrulis, E.D. *et al.* The RNA processing exosome is linked to elongating RNA polymerase II in *Drosophila*. *Nature* **420**, 837–841 (2002).
19. Basu, U. *et al.* The RNA exosome targets the AID cytidine deaminase to both strands of transcribed duplex DNA substrates. *Cell* **144**, 353–363 (2011).
20. Hessle, V. *et al.* The exosome associates cotranscriptionally with the nascent pre-mRNP through interactions with heterogeneous nuclear ribonucleoproteins. *Mol. Biol. Cell* **20**, 3459–3470 (2009).
21. Hieronymus, H., Yu, M.C. & Silver, P.A. Genome-wide mRNA surveillance is coupled to mRNA export. *Genes Dev.* **18**, 2652–2662 (2004).
22. Lim, S.J., Boyle, P.J., Chinen, M., Dale, R.K. & Lei, E.P. Genome-wide localization of exosome components to active promoters and chromatin insulators in *Drosophila*. *Nucleic Acids Res.* **41**, 2963–2980 (2013).
23. Castelnuovo, M. *et al.* Bimodal expression of *PHO84* is modulated by early termination of antisense transcription. *Nat. Struct. Mol. Biol.* **20**, 851–858 (2013).
24. Shah, S., Wittmann, S., Kilchert, C. & Vasiljeva, L. lncRNA recruits RNAi and the exosome to dynamically regulate pho1 expression in response to phosphate levels in fission yeast. *Genes Dev.* **28**, 231–244 (2014).
25. Wagschal, A. *et al.* Microprocessor, Setx, Xrn2, and Rrp6 co-operate to induce premature termination of transcription by RNAPII. *Cell* **150**, 1147–1157 (2012).
26. Yamanaka, S., Yamashita, A., Harigaya, Y., Iwata, R. & Yamamoto, M. Importance of polyadenylation in the selective elimination of meiotic mRNAs in growing *S. pombe* cells. *EMBO J.* **29**, 2173–2181 (2010).
27. Keller, C., Woolcock, K., Hess, D. & Buhler, M. Proteomic and functional analysis of the noncanonical poly(A) polymerase Cid14. *RNA* **16**, 1124–1129 (2010).
28. Vasiljeva, L. & Buratowski, S. Nrd1 interacts with the nuclear exosome for 3′ processing of RNA polymerase II transcripts. *Mol. Cell* **21**, 239–248 (2006).
29. West, S., Gromak, N., Norbury, C.J. & Proudfoot, N.J. Adenylation and exosome-mediated degradation of cotranscriptionally cleaved pre-messenger RNA in human cells. *Mol. Cell* **21**, 437–443 (2006).
30. Lebreton, A., Tomecki, R., Dziembowski, A. & Seraphin, B. Endonucleolytic RNA cleavage by a eukaryotic exosome. *Nature* **456**, 993–996 (2008).
31. Schaeffer, D. *et al.* The exosome contains domains with specific endoribonuclease, exoribonuclease and cytoplasmic mRNA decay activities. *Nat. Struct. Mol. Biol.* **16**, 56–62 (2009).
32. Wasmuth, E.V. & Lima, C.D. Exo- and endoribonucleolytic activities of yeast cytoplasmic and nuclear RNA exosomes are dependent on the noncatalytic core and central channel. *Mol. Cell* **48**, 133–144 (2012).
33. Nudler, E. RNA polymerase backtracking in gene regulation and genome instability. *Cell* **149**, 1438–1445 (2012).
34. Cheung, A.C. & Cramer, P. Structural basis of RNA polymerase II backtracking, arrest and reactivation. *Nature* **471**, 249–253 (2011).
35. Izban, M.G. & Luse, D.S. The RNA polymerase II ternary complex cleaves the nascent transcript in a 3′ → 5′ direction in the presence of elongation factor SII. *Genes Dev.* **6**, 1342–1356 (1992).
36. Mason, P.B. & Struhl, K. Distinction and relationship between elongation rate and processivity of RNA polymerase II *in vivo*. *Mol. Cell* **17**, 831–840 (2005).
37. Sigurdsson, S., Dirac-Svejstrup, A.B. & Svejstrup, J.Q. Evidence that transcript cleavage is essential for RNA polymerase II transcription and cell viability. *Mol. Cell* **38**, 202–210 (2010).
38. Churchman, L.S. & Weissman, J.S. Nascent transcript sequencing visualizes transcription at nucleotide resolution. *Nature* **469**, 368–373 (2011).
39. Birse, C.E., Lee, B.A., Hansen, K. & Proudfoot, N.J. Transcriptional termination signals for RNA polymerase II in fission yeast. *EMBO J.* **16**, 3633–3643 (1997).
40. Gómez-Herreros, F. *et al.* One step back before moving forward: regulation of transcription elongation by arrest and backtracking. *FEBS Lett.* **586**, 2820–2825 (2012).
41. Nielsen, S., Yuzenkova, Y. & Zenkin, N. Mechanism of eukaryotic RNA polymerase III transcription termination. *Science* **340**, 1577–1580 (2013).
42. Gusarov, I. & Nudler, E. Control of intrinsic transcription termination by N and NusA: the basic mechanisms. *Cell* **107**, 437–449 (2001).
43. Makino, D.L., Baumgartner, M. & Conti, E. Crystal structure of an RNA-bound 11-subunit eukaryotic exosome complex. *Nature* **495**, 70–75 (2013).
44. Somesh, B.P. *et al.* Multiple mechanisms confining RNA polymerase II ubiquitylation to polymerases undergoing transcriptional arrest. *Cell* **121**, 913–923 (2005).
45. Torchet, C. *et al.* Processing of 3′-extended read-through transcripts by the exosome can generate functional mRNAs. *Mol. Cell* **9**, 1285–1296 (2002).

ONLINE METHODS

Yeast strains, plasmids and media. A list of all *S. pombe* strains used in this study is provided in **Supplementary Table 1**. Cells were routinely grown at 30 °C in yeast extract medium with amino acid supplements (YES) or Edinburgh minimal medium (EMM) supplemented with appropriate amino acids. Conditional strains in which the genomic copy of *dis3*, *rrp41*, or *mtr4* is expressed from the thiamine-repressible *nmt1* promoter (P_{nmt1}) were generated as described previously[46]. P_{nmt1}-dependent expression was repressed by the addition of 60 μM thiamine to the growth medium for 12–15 h. For induction of *tfs1* expression and its derivative mutated version, an initial culture grown for 6 h in the presence of thiamine was split into two cultures supplemented with either 0.3% EtOH or 7.5 μM anhydrotetracycline hydrochloride (AhTET; Sigma-Aldrich, 94664) and allowed to grow for another 6 h. Gene disruptions and C-terminal tagging of proteins of interest were performed by PCR-mediated gene targeting[47] with the lithium acetate method for cell transformation. Knockout strains were confirmed by rt-PCR, and promoter swaps and protein tagging were validated by PCR screening and/or western blotting. Primer sequences used throughout this study are available upon request.

***ura4* reporter system for transcription termination defects.** Reporter constructs for *snR99* terminator activity were created with the *ade6* integration vector[46] with pFB366 as the host vector and contain 1 kb of *snR99* promoter sequences followed by the *ura4* coding region and an additional 0.5 kb of *ura4* 3′-UTR sequences, to result in pFB741. To address the impact of depleting Dis3 on transcription termination, a 332-nt region from the *snR99* terminator sequence[48] was cloned upstream of the *ura4* coding region of pFB741, to generate pFB745. Both constructs were confirmed by sequencing. For single integration into the *ade6* locus, pFB741 and pFB745 were linearized and transformed into FBY106 and FBY721 strains. Positive integrants were confirmed by PCR screening with primers located within the *ura4* coding region.

***ura4* construct with alteration in transcriptional pausing elements.** The *ura4* mutant defective in transcriptional pausing (*ura4* 3′ mutant) was generated by a multistep procedure beginning with the PCR-mediated deletion of the DSE element[39] from a genomic DNA fragment covering the *ura4* coding region and 0.5 kb of 3′ intergenic region with a 106-nt-long reverse primer that included 5′ and 3′ flanking DNA sequences of the 131-nt-long DSE element. The PCR product corresponding to DSE-deleted *ura4* was cloned downstream of *snR99* promoter sequences to generate pFB836. Deletion of SDE1 and mutations in SDE2 were performed as described previously[39], with PCR-based mutagenesis on pFB836, to result in pFB881. All constructs were confirmed by DNA sequencing. For single integration into the *ade6* locus, pFB741 (*ura4* 3′ WT) and pFB881 (*ura4* 3′ mutant) were linearized and transformed into FBY106 and FBY721 strains. Positive integrants were confirmed by PCR screening with primers located within the *ura4* coding region.

Tfs1 expression constructs. To generate the Tfs1 expression constructs, the *tfs1* coding region was PCR amplified from cDNA and cloned into the tetracycline-inducible expression vector $pMLtet^{ON}$ (a generous gift of M. Luetzelberger) (pFB789), to result in pFB811. Plasmid $pMLtet^{ON}$ was constructed by replacement of the *nmt1* promoter in pML11 (described below; located between PstI and AgeI) with a DNA fragment carrying the $CaMV35Stet^{ON}$ promoter and *tet* repressor, which was PCR amplified from pDUAL-tetR-rpsL-neo[49]. In order to obtain unique restriction sites within the MCS of $pMLtet^{ON}$, two restriction sites (BamHI and SphI), were subsequently removed from the pDUAL fragment by site-directed mutagenesis. Plasmid pML11 was constructed by insertion of a new MCS (PstI-NdeI-AgeI-SphI-BamHI-SalI-SpeI-MluI-SmaI-SacI) into the PstI–SacI site of pJK148. Subsequently, the *nmt1* promoter and terminator sequences of pREP2 (ref. 50) were ligated into the PstI–NdeI and SmaI–SacI sites of the new MCS, respectively. The mutated version of *tfs1* was created by site-directed mutagenesis with pFB811 as template changing Asp274 and Glu275 to alanine residues. All constructs were confirmed by DNA sequencing.

Dis3 expression constructs. To generate the Dis3 expression constructs, the coding region of *dis3* with an additional 0.5 kb of promoter and terminator sequences was PCR amplified from genomic DNA and cloned into pFB366, to result in pFB693. Endoribonucleolytic (endo$^-$) and exoribonucleolytic (exo$^-$) mutant versions of Dis3 were generated by site-directed mutagenesis with pFB693 as template to change Asp166 and Asp516 to asparagine residues and result in pFB702 (endo$^-$) and pFB707 (exo$^-$), respectively. A catalytically inactive version of Dis3 impaired in both enzymatic activities (endo$^-$ exo$^-$) was also generated (pFB708). All constructs were confirmed by sequencing. For single integration into the *ade6* locus, pFB366, pFB693, pFB702, pFB707 and pFB708 were linearized and transformed into the conditional P_{nmt1}-dis3 strain (FBY721). Positive integrants were confirmed by growth selection on EMM agar plates lacking adenine.

Rrp41 expression constructs. To generate the wild-type (WT) Rrp41 expression construct, the *rrp41* coding region plus 0.5 kb and 0.65 kb of 5′ and 3′ genomic sequences, respectively, was PCR amplified with genomic DNA, and the PCR product was cloned into the *ade6* integration vector pFB366, to result in pFB855. The *rrp41* expression construct bearing a channel-occluding (co) insertion was created by a two-step procedure beginning with the cloning of a PCR-amplified genomic fragment containing 0.5 kb of *rrp41* 5′-UTR sequences and the first 345 bp of the *rrp41* coding region (fragment 1, amino acids 1–62); this was followed by the cloning of a second DNA fragment containing nucleotides 346–888 of the *rrp41* coding region (amino acids 63–242) plus 0.65 kb of 3′-UTR sequences (fragment 2). The DNA sequence encoding the channel-occluding insertion was included in the 3′ primer used to amplify fragment 1. This procedure inserted an exogenous PstI site between nucleotides 345 and 346, which was subsequently changed to an XhoI site by site-directed mutagenesis to generate the final channel-occluding insertion N-GESEGESEGLE-C (pFB955). This insertion is similar in length and in amino acid composition to a previously described insertion known to physically occlude the central channel of the *S. cerevisiae* RNA exosome[32]. The wild-type and channel-insertion Rrp41 expression constructs were confirmed by sequencing. For single integration into the *ade6* locus, pFB366, pFB855 and pFB955 were linearized and transformed into the conditional P_{nmt1}-rrp41 strain (FBY1347). Positive integrants were confirmed by growth selection on EMM agar plates lacking adenine.

RNA preparation and analyses. Total yeast RNA was extracted with the hot-acid phenol method, was resolved on agarose-formaldehyde gels or on polyacrylamide-urea gels in RNase H experiments and was subsequently transferred onto nylon membranes before RNAs cross-linking. Prehybridization and overnight hybridization were carried out in Church buffer at 42 °C and 65 °C for DNA and RNA probes, respectively. Strand-specific RNA probes used for northern analyses were designed to be complementary to ORF sequences. RNA probes were generated by *in vitro* transcription with the T7 riboprobe system (Ambion) and internally labeled with [α-^{32}P]UTP. DNA probes were generated by 5′-end labeling of single-stranded oligonucleotides with the T4 polynucleotide kinase and [γ-^{32}P]ATP. For DNA probes, 2 × 15 min washes in 2× SSC and 0.1% SDS, and 2 × 5 min washes in 0.1× SSC and 0.1% SDS were performed; for RNA probes, 3 × 15 min washes in 1× SSC and 0.1% SDS, and one 15 min wash in 0.1× SSC and 0.1% SDS were performed. Membranes were exposed with Phosphor Screens, and this was followed by visualization and quantification of signals with a Typhoon Trio instrument and ImageQuant TL, respectively (GE Healthcare). rt-PCR analyses were done as previously described[48].

RNase H cleavage assays. Total yeast RNA was treated by RNase H as previously described[48] with a mixture containing DNA oligonucleotides complementary to sequences downstream of the snR3 polyadenylation sites (as illustrated in **Supplementary Fig. 1c**) in order to detect snR3 readthrough transcripts. Annealing of these antisense DNA oligonucleotides to 3′-extended snR3 transcripts (3′ ext) resulted in RNA–DNA hybrids that were cleaved by RNase H to release a specific RNA fragment that was detected with a strand-specific riboprobe complementary to this RNase H–cleaved product.

Protein analysis. Total cell extracts were prepared by harvesting mid-log cells in ice-cold lysis buffer (50 mM Tris, pH 7.5, 5 mM $MgCl_2$, 150 mM NaCl and 0.1% NP-40) containing a cocktail of protease inhibitors (PMSF and PLAAC) before glass-bead lysis with a Fastprep instrument. Clarified lysates were normalized for total protein concentration with the Bradford protein assay. For affinity-purification experiments, 2 mg of total proteins were subjected to immunoprecipitation with 50 μl of 50% slurry IgG-Sepharose beads that were preequilibrated in lysis buffer, and gently mixed for 2 h. The beads were then washed three times with 1 ml of lysis buffer, and the bound proteins were eluted in SDS-PAGE sample buffer. Proteins were separated by SDS-PAGE, transferred to nitrocellulose membranes, and analyzed by immunoblotting with a rabbit polyclonal antibody

specific to Dis3 (ref. 51) (B-Bridge, 63-123; 1:500 (v/v) dilution), a mouse monoclonal antibody specific to α-tubulin (Sigma-Aldrich, T5168; 1:1,000 (v/v) dilution), and a rabbit polyclonal antibody against protein A (Sigma-Aldrich, P3775; 1:10,000 (v/v) dilution) in the case of TAP-tagged proteins. Validation is provided on the manufacturer's website for the antibodies against α-tubulin and protein A. Membranes were then probed with donkey anti-rabbit antibody conjugated to IRDye 800CW (LI-COR, 926-32213; 1:15,000 (v/v) dilution) and a goat anti-mouse antibody conjugated to AlexaFluor 680 (Life technologies, A-21057; 1:15,000 (v/v) dilution). Detection of the proteins was performed with an Odyssey infrared imaging system (LI-COR).

Chromatin immunoprecipitation (ChIP) assays. ChIP experiments were performed essentially as described[52]. For ChIP-seq experiments, chromatin immunoprecipitation was done as described above with the following modifications. We scaled up the reactions to obtain a larger amount of chromatin for library preparation. Chromatin was immunoprecipitated with Pan mouse IgG Dynabeads (Life Technologies, 11041) coated with antibody against Rpb1 (8WG16, Covance MMS-126R) or anti-HA 12CA5 (Roche, 11 583 816 001) for the Rpb3-HA strain[10]. The 8WG16 antibody is known to recognize the C-terminal domain (CTD) of Rpb1 and measures total RNAPII along genes in yeast[53]. Control ChIP assays with untagged strains were performed for all experiments.

Transcription run-on assays. Transcription run-on experiments were performed essentially as described previously[54] with some modifications. Briefly, 150 ml of yeast cell cultures were grown in EMM supplemented with appropriate amino acids and 60 μM of thiamine for 15 h to an OD_{600} of 0.20–0.25. Cells were collected by centrifugation, washed with ice-cold water and resuspended in 950 μl of ice-cold water. *N*-lauryl sarcosine sulfate (sarkosyl) was added to a final concentration of 0.5%, and cells were incubated on ice for 20 min. Cells were recovered by low-speed centrifugation, and the supernatant was removed. Cells were then resuspended in 60 μl of 2.5× transcription buffer (50 mM Tris-HCl, pH 7.7, 500 mM KCl, and 80 mM $MgCl_2$) containing 2 mM DTT, 2 mM each ATP, CTP and GTP and 100 μCi of [α-^{32}P]UTP in a final volume of 150 μl. Transcription was allowed to proceed for 10 min at 30 °C before cells were washed with water and total RNA extraction was performed. After partial RNA hydrolysis with 0.2 M NaOH on ice for 5 min, RNA was neutralized with 0.14 M Tris, and 0.14 M HCl. Single-stranded RNA probes were generated by *in vitro* transcription with a T7 RNA polymerase, and 1 μg of each probe was immobilized on Hybond-XL (GE Healthcare) membranes by slot-blotting. Membranes were prehybridized overnight in 50% formamide, 5× SSPE, 5× Denhart's, 0.4% SDS, and 100 μg/ml salmon sperm DNA at 45 °C. Hybridizations were performed for 24 h at 45 °C after the addition of denatured radiolabeled RNA with 12 mm × 75 mm tubes containing 2 ml of 9% dextran sulfate, 50% formamide, 5× SSPE, 1× Denhart's, 0.4% SDS and 100 μg/ml salmon sperm DNA. Membranes were washed two or three times for 5 min in a large volume of 2× SSC and 0.1% SDS at 45 °C. Membranes were exposed with Phosphor Screens, and this was followed by visualization and quantification of signals with a Typhoon Trio instrument and ImageQuant TL, respectively. Signal values for each probe were corrected for background signal in a *ura4* ORF region, because all strains used in the run-on assays had a deletion of the *ura4* coding region (*ura4-D18* allele).

Growth assays. For growth assays, 50 μl of appropriated early-log-phase cell suspensions (OD_{600} of 0.02) with episomally maintained pFB789, pFB811 or pFB818 were added to 50 μl of EMM Leu$^-$ medium or 50 μl of EMM Leu$^-$ medium supplemented with 7.5 μM (final concentration) of the nonmetabolic inducer anhydrotetracycline hydrochloride (AhTET). Samples were prepared in triplicate in Costar 96-well noncoated polystyrene microplates, and cell growth was monitored with a PowerWave microplate spectrophotometer reader (BioTek Instruments) with software settings previously described[55]. For spot assays, exponential cell cultures were adjusted to an optical density OD_{600} of 1.0, and then 3 μl of ten-fold serial dilutions of the suspension were spotted on the appropriated plates. Plates were incubated for 3–5 d at 30 °C.

Library preparation and Illumina sequencing. Libraries were prepared from total *S. pombe* RNA and sequenced with Illumina HiSeq technology. Libraries for RNA-seq analysis were generated as described in ref. 46. For ChIP-seq analyses, libraries were prepared with the NEBNext ChIP-Seq Library Prep Master Mix Set for Illumina kit (New England BioLabs) according to the manufacturer's instructions.

RNA-seq data analysis. Raw FASTQ file quality was assessed with the FastQC software (http://www.bioinformatics.babraham.ac.uk/projects/fastqc/). Raw reads were mapped and processed, and raw read numbers per feature were extracted as described[46]. Fission-yeast genome annotation as available on 9 May 2011 was used throughout this study. Sequencing scores for each base (number of reads mapping to a given nucleotide position divided by total number of mapped reads) were calculated. RNA-seq scores were displayed along genome annotation with the Bioconductor 'tilingarray' package[56]. Poly(A)-cleavage sites were identified for 792 genes with the approach described by Schlackow *et al.*[57]. Briefly, reads containing stretches of at least four As at their 3′ end were selected. Reads containing poly(A) stretches encoded in the genome were filtered out. Poly(A)-cleavage sites less than 6 nt apart were collapsed into one site. Poly(A) sites were assigned to the nearest upstream annotated gene. For each gene, the poly(A) site with the most hits was defined as 'main', whereas the one furthest away from the ORF defines the 'longest UTR'. Signal accumulation values around poly(A)-cleavage sites were calculated as the number of normalized sequence hits per nucleotide over a fixed distance on either side of the main poly(A) site of these 792 genes. Only genes ($n = 792$) for which poly(A)-cleavage sites could be mapped in the wt.2_rna sample have been used for this analysis. Data were median-centered for representation. Differential gene-expression analyses in coding (ORF for mRNAs and mature transcripts for snoRNAs and snRNAs) and downstream regions (500 nt downstream of TTSs, as annotated in Pombase[58]) were performed with raw mapped read numbers and the DESeq Bioconductor package[59] with samples wt.1_rna and wt.2_rna as untreated samples.

ChIP-seq data analysis. Raw reads were mapped and processed as for RNA-seq experiments except that the data were not treated as strand specific. Data for each pulldown (IP) were normalized with data from input chromatin (IN) as follows. Sequencing scores for each base (number of reads mapping to a given nucleotide position divided by total number of mapped reads) were calculated. The mean sequencing score in a 10-nt window centered around each IP nucleotide was computed and divided by the corresponding mean score calculated for the IN sample. Normalized data were then median-centered and used for subsequent analysis. Chip-seq data were displayed along genome annotation with jBrowse[60]. Read accumulation 500 nt upstream and 500 nt downstream of the poly(A)-cleavage sites mapped for the aforementioned 792 genes was calculated as for the RNA-seq data. Average gene analyses were performed on normalized data with custom R scripts (flanking region = 500 nt split into ten bins; genes split into 20 bins) and with gene coordinates (including 5′ and 3′ UTRs when available) as annotated in Pombase[58].

46. Lemieux, C. *et al.* A Pre-mRNA degradation pathway that selectively targets intron-containing genes requires the nuclear poly(A)-binding protein. *Mol. Cell* **44**, 108–119 (2011).
47. Bähler, J. *et al.* Heterologous modules for efficient and versatile PCR-based gene targeting in *Schizosaccharomyces pombe*. *Yeast* **14**, 943–951 (1998).
48. Lemay, J.F. *et al.* The nuclear poly(A)-binding protein interacts with the exosome to promote synthesis of noncoding small nucleolar RNAs. *Mol. Cell* **37**, 34–45 (2010).
49. Erler, A., Maresca, M., Fu, J. & Stewart, A.F. Recombineering reagents for improved inducible expression and selection marker re-use in *Schizosaccharomyces pombe*. *Yeast* **23**, 813–823 (2006).
50. Maundrell, K. Thiamine-repressible expression vectors pREP and pRIP for fission yeast. *Gene* **123**, 127–130 (1993).
51. Kinoshita, N., Goebl, M. & Yanagida, M. The fission yeast dis3+ gene encodes a 110-kDa essential protein implicated in mitotic control. *Mol. Cell. Biol.* **11**, 5839–5847 (1991).
52. Larochelle, M., Lemay, J.F. & Bachand, F. The THO complex cooperates with the nuclear RNA surveillance machinery to control small nucleolar RNA expression. *Nucleic Acids Res.* **40**, 10240–10253 (2012).
53. Bataille, A.R. *et al.* A universal RNA polymerase II CTD cycle is orchestrated by complex interplays between kinase, phosphatase, and isomerase enzymes along genes. *Mol. Cell* **45**, 158–170 (2012).
54. Gullerova, M. & Proudfoot, N.J. Cohesin complex promotes transcriptional termination between convergent genes in S. pombe. *Cell* **132**, 983–995 (2008).
55. Toussaint, M. & Conconi, A. High-throughput and sensitive assay to measure yeast cell growth: a bench protocol for testing genotoxic agents. *Nat. Protoc.* **1**, 1922–1928 (2006).
56. Huber, W., Toedling, J. & Steinmetz, L.M. Transcript mapping with high-density oligonucleotide tiling arrays. *Bioinformatics* **22**, 1963–1970 (2006).
57. Schlackow, M. *et al.* Genome-wide analysis of poly(A) site selection in *Schizosaccharomyces pombe*. *RNA* **19**, 1617–1631 (2013).
58. Wood, V. *et al.* PomBase: a comprehensive online resource for fission yeast. *Nucleic Acids Res.* **40**, D695–D699 (2012).
59. Anders, S. & Huber, W. Differential expression analysis for sequence count data. *Genome Biol.* **11**, R106 (2010).
60. Skinner, M.E., Uzilov, A.V., Stein, L.D., Mungall, C.J. & Holmes, I.H. JBrowse: a next-generation genome browser. *Genome Res.* **19**, (2009).

doi:10.1038/nsmb.2893